atmosphere

MDPI

Article

Extreme Temperature Index in China from a Statistical Perspective: Change Characteristics and Trend Analysis from 1961 to 2021

Xulei Wang, Lifeng Wu * and Huiying Liu

School of Water Conservancy and Ecological Engineering, Nanchang Institute of Technology, Nanchang 330099, China; 2022301005@nit.edu.cn (X.W.); huiyingliu@nit.edu.cn (H.L.)
* Correspondence: 2015994554@nit.edu.cn

Abstract: Against the backdrop of intensified global climate change, the frequency and intensity of extreme weather events in mainland China continue to rise due to its unique topography and complex climate types. In-depth research on the trends and impacts of climate extremes can help develop effective adaptation and mitigation strategies to protect the environment and enhance social resilience. In this research, temperature data from 2029 meteorological stations for the period 1961–2021 were used to study 15 extreme temperature indices and 3 extreme composite temperature indices. Linear propensity estimation and the Mann–Kendall test were applied to analyze the spatial and temporal variations in extreme temperatures in China, and Pearson's correlation analysis was used to reveal the relationship between these indices and atmospheric circulation. The results show that in the past 60 years, the extreme temperature index in China has shown a trend of decreasing low-temperature events and increasing high-temperature events; in particular, the increase in warm nights is significantly higher than that of warm days. In terms of spatial distribution, daily maximum temperature less than the 10th percentile (TX10P) and daily minimum temperature greater than the 90th percentile (TN90P) increased significantly in the warm temperate sub-humid (WTSH) region, north subtropical humid (NSH) region, and marginal tropical humid (MTH) region, whereas frost days (FD0) and diurnal temperature range (DTR) decreased significantly. In the extreme composite temperature index, extreme temperature range (ETR) showed a downward trend, while compound heatwave (CHW) and compound heatwave and relative humidity (CHW-RH20) increased, with the latter mainly concentrated in the WTSH and NSH regions. Correlation analysis with climate oscillation shows that Arctic Oscillation (AO), Atlantic Multiannual Oscillation (AMO), and El Niño–Southern Oscillation (ENSO) are positively correlated with extremely high temperatures, whereas North Atlantic Oscillation (NAO) and Pacific Decadal Oscillation (PDO) are negatively correlated.

Keywords: extreme composite temperature index; China region; space–time change; climate oscillation; Mann–Kendall test

Citation: Wang, X.; Wu, L.; Liu, H. Extreme Temperature Index in China from a Statistical Perspective: Change Characteristics and Trend Analysis from 1961 to 2021. *Atmosphere* **2024**, *15*, 1398. https://doi.org/10.3390/atmos15111398

Academic Editors: Yang Yu, Lei Wang and Cun Chang

Received: 21 September 2024
Revised: 16 October 2024
Accepted: 18 November 2024
Published: 20 November 2024

1. Introduction

Climate change is currently a serious challenge for humankind, with extreme weather being one of the most significant risks facing the world in both the short and long term [1]. The report of the 20th Party Congress pointed out that timely and accurate analysis and prevention of extreme weather and the all-round protection of people's lives and safety are the primary tasks of high-quality meteorological development [2]. The United Nations Intergovernmental Panel on Climate Change (IPCC) outlined in its Sixth Assessment Report that the occurrence of various extreme weather events has caused water and food crises for millions of people, with such phenomena being extremely prominent in Asia, Africa, and other regions [3]. Under the dual background of the impacts of human activities and global warming, extreme climate events have shown new trends of increasing frequency, increasing harm, and growing time, which have posed great challenges to the production

and development of human societies, the safety of life and property, and the stability of ecosystems [4–6]. A developing country with a population of 1.4 billion, China has complex and diverse topography and climate types, making it a sensitive and significant impact area of global climate change. This has deeply affected agricultural development, food security, infrastructure security, water resources, and natural ecosystems [7–9].

Extreme-temperature events are usually defined as low-probability events with significant damage that occur when the daily maximum or minimum temperature exceeds a specified threshold within a certain period of time, mainly including extremely high temperatures and extreme cold waves [10]. Since 2008, a number of relevant studies have proved that the morbidity and mortality caused by extreme-temperature events have continued to increase [11–13]. Long-term exposure to extremely high temperatures not only causes the most common symptoms of heat stroke, such as fainting, vomiting, and shock, but also leads to decreased attention and short-term memory impairment, accompanied by acute heart failure, chronic cardiovascular and cerebrovascular diseases, and respiratory diseases [14]. Long-term exposure to low-temperature and cold-wave environments causes the body to dissipate more heat than the body produces, which results in heat loss and increases the occurrence of low back pain, arthritis, rheumatism, and frostbite, and indirectly induces hypertension, pneumonia, myocardial infarction, and other diseases [15]. In addition, extreme-temperature events can cause a series of serious consequences such as increased power loss, infrastructure disruptions, food supply difficulties, paralysis of medical systems, communication signal failure, and even global economic crises [16–18].

Extreme-temperature events have attracted widespread attention from governments and meteorologists worldwide, becoming a current research hotspot. The research scales include the global, national, and watershed levels, among which the 16 extreme temperature indices recommended by the World Meteorological Organization (WMO) are the most widely used [19–23]. Zhang et al. found that in the past 50 years, over 70% of the global land area has experienced a significant increase in the number of warm nights and days, while the number of cold days and nights has significantly decreased, with the reduction in the extreme cold index being greater than the increase in the extreme warm index [24]. Lucas et al. studied the extreme climate index of the Xingu River Basin in Brazil and found that its extreme temperature index showed a significant upward trend [25]. Brown et al. showed that since 1950, global nighttime extreme high-temperature events have increased significantly, while extreme low-temperature events have decreased significantly, and the average daily temperature difference has been in a decreasing trend [26]. Kalyan et al. found that the extreme temperatures in the Gomati River basin in northern India have generally risen [27]. At the regional scale, there is significant consistency in extreme temperature index changes in regions such as the Asia–Pacific region, Saudi Arabia, Central and North South America, the Middle East, and Canada [28–30]. Many scholars in China have conducted extensive research on the Yangtze River Basin, Yellow River Basin, and provinces and municipal administrative regions. Zhang Ning et al. studied meteorological data from 234 stations in China from 1955 to 2005, and the results showed a clear upward trend in China's annual and seasonal extreme low temperatures, with the increase in extreme low temperatures being significantly larger than that of extreme high temperatures [31]. The extreme temperatures in all four seasons had varying degrees of warming trends, with the warming amplitude being particularly acute in winter. Chen et al. quantified the detectable impact of extreme summer heat in China based on data from 372 stations from 1960 to 2016, against the backdrop of global warming of 0.5 °C in the past [32]. The research results indicate that global warming has contributed to the emergence and prevalence of complex extreme high temperatures (continuous hot day and night). In southeastern China, the lower reaches of the Yangtze River, and northern China, the frequency of extreme high temperatures has increased by 2–4 times, and the duration and intensity have increased by 2–3 times. Zheng et al. investigated the spatiotemporal variations in heatwaves in northern China over the past 60 years, focusing on the heatwave events that occurred from 1961 to 2020 [33]. The results indicate that, on a time scale, the frequency, duration, and intensity

of heatwaves have shown a significant increasing trend. From the perspective of the spatial distribution, heatwave-prone areas are concentrated in the central and northern parts of the study area, with a greater increasing trend in Inner Mongolia, Gansu, and Xinjiang, while heatwave events rarely occur in Anhui and northern Jiangsu. Over the past half a century, heatwave events in northern China have shown an increasing trend year by year with a high degree of consistency in both time and space. Zhang et al. established a temperature series dataset for 10 cities in the Yangtze River Basin from 1901 to 2020 based on daily meteorological records from the early 20th century [34]. Research has found that in the past 40 years, the annual average temperature in these cities has significantly increased. In the past 120 years, the temperature rise trend in Chongqing and Shanghai has been particularly significant, with Shanghai experiencing greater warming than Chongqing, and the trend of change in Shanghai over the past 40 years is even more pronounced. In addition, the changes in regional extreme-temperature events are not only affected by global warming but are closely related to the urbanization process and the multi-annual variability of the East Asian monsoon. Zhang et al. found that extreme high-temperature events have increased significantly in most areas of the Yangtze River Basin over the past 60 years, especially since the 21st century, and the comprehensive risk of extreme climate events has continued to rise [35]. Sun et al. analyzed the spatial and temporal distribution characteristics of extreme-temperature events in Sichuan Province, and the research showed that their extreme value index and the numbers of high-temperature days, warm days, and warm-night days in Sichuan Province all showed a significant upward trend, while the numbers of frost days, cold days, and cold-night days showed a gradual downward trend [36]. Gegen et al., using temperature and precipitation data from the Qaidam Basin from 1960 to 2014, found that the extreme temperatures generally exhibited a significant warming trend, with the magnitude of change gradually decreasing from west to east [37]. Significant periods of freezing and growing season days also showed a lengthening trend. Overall, the extreme warm index showed a clear upward trend, while the extreme cold index showed a downward trend, but there were still significant spatial differences in different regions.

Among the different types of extreme-temperature events, the frequency and intensity of extreme heat events have significantly increased globally, closely related to anthropogenic global warming [38]. The above conclusions regarding changes in extreme heat were mainly based on univariate indices. Extreme heat usually refers to events where the maximum temperature during the day or the minimum temperature at night exceeds the 90th percentile [39]. According to this definition, hot days and hot nights should only occur during the day and night, respectively. However, definitions based on a single variable may not be able to identify the expected hot days and nights. If the maximum and minimum temperatures on a certain day exceed the set threshold, then that day can be defined as an extreme high-temperature day, more precisely a compound of daytime and nighttime heat [40]. There are significant differences in the mechanisms and impacts of similar compound extremes and independent hot days or nights, with individual daytime extreme high temperatures interfering with the normal functioning of human society and ecosystems, which may be mitigated by the arrival of subsequent cool nights. Even when the temperature is lower during the day, extremely hot nights can still cause an imbalance in human temperature regulation [41]. Compound extremes combine and amplify the adverse effects of day and night extremes, which may pose a serious threat.

China has a vast territory, covering various landforms and climate types from the cold northeast to the hot south, as well as plateaus and plains. Studying extreme temperatures in the region can help to understand the challenges and impacts of different regions when facing extreme weather events. Although a large number of studies have been conducted, most of them are limited to local areas and conventional extreme temperature indices, and the research results cannot accurately reflect the complex climate change characteristics of the entire study area. Therefore, this study used 15 extreme temperature indices from the 27 extreme climate indices released by the WMO to analyze the entire

Chinese mainland region. On this basis, three composite extreme temperature indices were also proposed. Careful classification can provide a more detailed assessment of changes in extreme temperatures and further improve and enrich previous conclusions. The research results not only comprehensively reveal the characteristics of and trends in extreme-temperature events on the Chinese mainland but also have practical significance for predicting and preventing climate disasters.

2. Materials and Methods

2.1. Overview of the Study Area

China is located in the eastern part of Asia, at longitudes 73°33 E to 135°05 E and latitudes 18°03 N to 53°33 N, with a total land area of approximately 9.6 million km^2. The eastern part of the country is bordered by the sea, the western part is characterized by mountainous and highland terrain, the central part has plains, the southern part has a tropical and subtropical climate, and the northern part has a temperate and cold climate. This geographical and climatic diversity causes China to show significant differences in its extreme temperatures.

The whole Chinese mainland can be divided into seven major climatic regions to analyze the temperature changes and trends in different regions in more detail. These include the middle temperate arid (MTA) region, plateau temperate semi-arid (PTSA) region, middle temperate semi-arid (MTSA) region, middle temperate semi-humid (MTSH) region, warm temperate semi-humid (WTSH) region, northern subtropical humid (NSH) region, and marginal tropical humid (MTH) regions. These regions have different climate characteristics.

The middle temperate arid region is mainly characterized by low annual precipitation and high evaporation. The climate is characterized by cold winters and hot summers, with large temperature differences between day and night and between years. They are mainly distributed across northern Xinjiang and western Inner Mongolia.

The plateau temperate semi-arid region refers to a relatively high plateau area with a mild but dry climate and moderate but unevenly distributed annual rainfall, mainly distributed in some areas of the Qinghai–Tibet Plateau, such as the eastern part of the Qaidam Basin and the Qiangtang cold desert area.

The middle temperate semi-arid region is mainly distributed in the middle east of the Inner Mongolian Plateau and parts of the Loess Plateau with less annual precipitation. The climatic characteristics of these areas vary from dry to wet. The annual precipitation is less but relatively uniform, and the vegetation is dominated by grasslands and shrubs.

The middle temperate semi-humid region is mainly distributed in the eastern part of the Inner Mongolian Plateau, where the annual precipitation is between 400 and 800 mm. The climate in these areas is characterized by four distinct seasons, cold winters, warm summers, relatively moderate precipitation, and neither extreme drought nor extreme humidity.

The warm temperate semi-humid region has a mild climate, moderate annual precipitation, and a relatively uniform seasonal distribution, which is conducive to agricultural production, mainly in eastern and central China, such as the North China Plain in northern China.

The northern subtropical humid region has a warm and humid climate, rich annual precipitation, and clear seasonal changes. It is characterized by evergreen broad-leaved forest and deciduous broad-leaved forest and is located in the south of the Qinhuai Line, including the Hanjiang River basin in Shaanxi, the Middle and Lower Yangtze Valley Plain, and most areas of the Jianghuai Plain.

The marginal tropical humid region is hot and rainy, with high and evenly distributed precipitation, mainly consisting of tropical rainforests and monsoon forests, mainly distributed in the southernmost areas of China, such as Hainan Island, Leizhou Peninsula, and southern Taiwan Province.

East and South China experience high-temperature heatwave events in summer, while Northwest China may also experience extremely high temperatures, and North, Northeast, and Northwest China may experience low-temperature cold waves, even in

winter. The frequent occurrence of extreme-temperature events has become a problem that cannot be ignored, not only posing a serious threat to China's industrial layout and urban development but also directly affecting people's health and wellbeing. Therefore, understanding China's geographical and climatic diversity is crucial for analyzing changes in extreme temperature indices and regional differences.

2.2. Data Sources

This study focuses on extreme-temperature events in China, using meteorological data sourced from the China Meteorological Data Network (http://data.cma.cn/ accessed on 4 July 2024), with the daily measured maximum and minimum temperatures at each station from 1961 to 2021 serving as the dataset. To further ensure the accuracy and reliability of the data, the dataset was first preprocessed: (1) the time scale of the selected site data was not less than 61 years; (2) if the T_{max} or T_{min} data of a site were missing more than 5% of the total or if data were lost for 30 consecutive days, the site was not selected; (3) data quality control was conducted using the RclimDex1.1 editor program [42], and unreasonable data, such as multiple consecutive days with the same temperature, cases where the lowest temperature exceeded the highest temperature, and recorded values seriously deviating from the actual meteorological conditions of the region (i.e., values exceeding 3 times the standard deviation, defined as out-of-bounds values), were treated as missing measurement values. Linear interpolation was used to interpolate outliers and missing values for a very small number of sites. A total of 2029 meteorological stations with good spatial representativeness, consistent data age, and high data completeness were selected from seven climate regions within the study area (Figure 1).

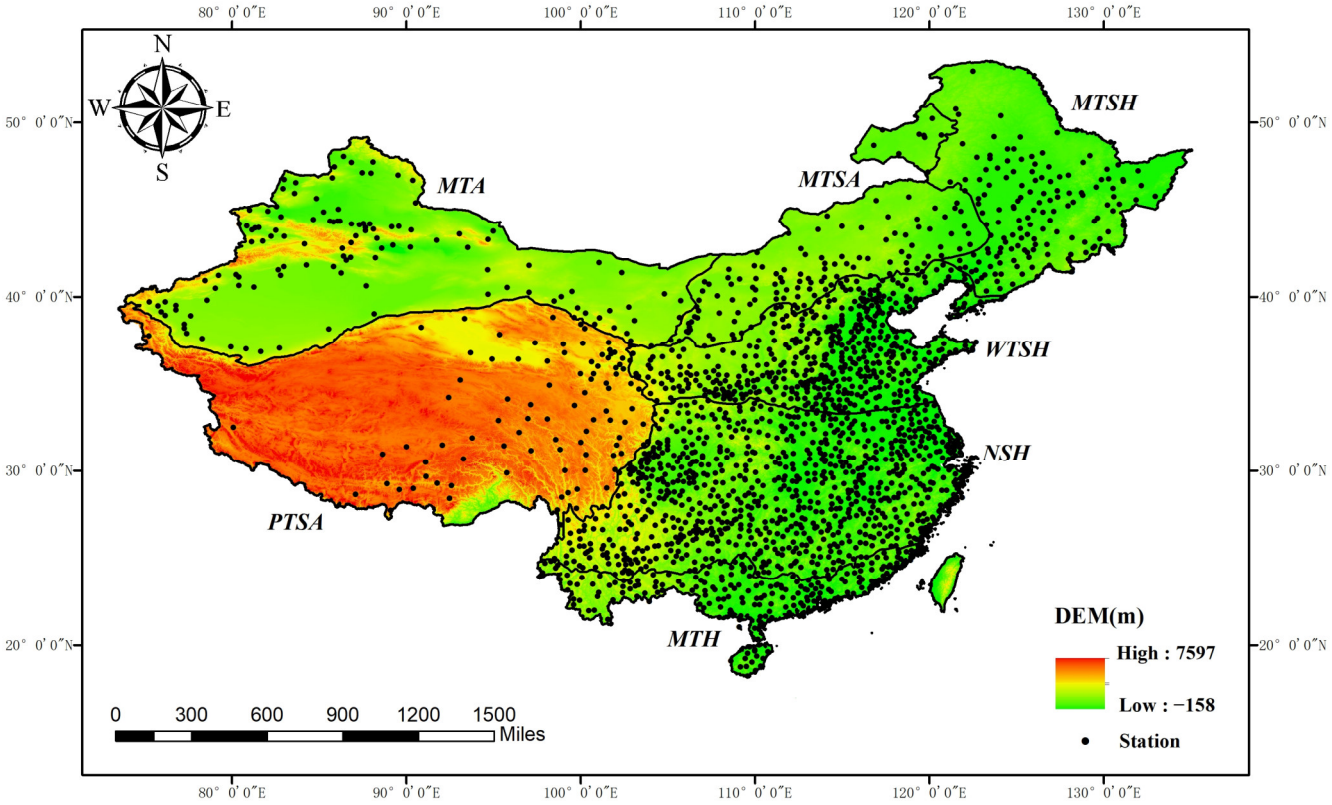

Figure 1. Climate zoning and distribution of meteorological stations on the Chinese mainland.

To further explore the relationship between extreme temperature indices and climate oscillations, this study focused on analyzing a variety of representative large-scale climate indices. These indices include the Arctic Oscillation (AO), Atlantic Multiannual Oscillation (AMO), El Niño–Southern Oscillation (ENSO), North Atlantic Oscillation (NAO), and

Pacific Decadal Oscillation (PDO). These climate indices quantify changes in atmospheric circulation patterns, with the relevant data obtained from the National Weather Service Climate Prediction Center (https://www.cpc.ncep.noaa.gov/products/precip/CWlink/MJO/climwx.shtml accessed on 21 July 2024). The data contained detailed climate data and a trend analysis, as listed in Table 1. By analyzing the correlation between indices, we can gain a more comprehensive understanding of the interrelationships between extreme temperatures and these large-scale climate factors and reveal their mechanisms of action under different climate conditions.

Table 1. Details of data for different large-scale climate indices.

Climatic Index	Index Code	Time Span (Year-Month)	Description
Arctic Oscillation	AO	1961.01–2021.12	The dominant mode of atmospheric ring rheology in the tropical outer regions of the Northern Hemisphere
Atlantic Multiannual Oscillation	AMO	1961.01–2021.12	Annual mean of sea surface temperature anomalies in the region (75–7.5° W, 0°–60° N)
El Niño–Southern Oscillation	ENSO	1961.01–2021.12	Average sea surface temperature anomaly in the region (5° N–5° S, 120° W–170° W)
North Atlantic Oscillation	NAO	1961.01–2021.12	Normalized sea level pressure difference between the Azores and Iceland
Pacific Decadal Oscillation	PDO	1961.01–2021.12	Time coefficient of the first mode after EOF of monthly SST north of 20° N Pacific Ocean

2.3. Research Methods

To quantitatively characterize the spatial and temporal characteristics of extreme-temperature events in mainland China, this study selected 15 widely used extreme temperature indices from the 27 extreme climate indices recommended by the International Panel on Climate and Indicators (ETCCDI) and proposed 3 new extreme composite temperature indices [43]. The definitions and codes of each index are listed in Table 2. Each index was calculated using the clinmDex1.1 package of RStudio software (version R 4.4.1. lnk). The linear tendency estimation method was used to calculate and analyze the trend of extreme-temperature events in the time series. The Mann–Kendall (M-K) statistical test was used to test the significance of the indices, and ArcGIS technology was incorporated to visualize the spatial trend of extreme-temperature events. Finally, the correlation between the extreme temperature index and atmospheric circulation was explored to reveal its potential impact and mechanism.

Table 2. Definition and classification of extreme temperature indices.

Classification	Name	Description	Index Code	Units
Relative index	Cool days	Percentage of time when daily min temperature < 10th percentile	TX10P	d
	Cool nights	Percentage of time when daily min temperature < 10th percentile	TN10P	d
	Warm days	Percentage of time when daily max temperature > 90th percentile	TX90P	d
	Warm nights	Percentage of time when daily min temperature > 90th percentile	TN90P	d

Table 2. *Cont.*

Classification	Name	Description	Index Code	Units
Absolute Index	Frost days	Annual count when daily minimum temperature < 0 °C	FD0	d
	Ice days	Annual count when daily maximum temperature < 0 °C	ID0	d
	Summer days	Annual count when daily max temperature > 25 °C	SU25	d
	Tropical nights	Annual count when daily min temperature > 20 °C	TR20	d
Extreme Value Index	Hottest day	Monthly and annual highest value of daily max temperature	TXx	°C
	Warmest night	Monthly and annual highest value of daily min temperature	TNx	°C
	Coldest day	Monthly and annual lowest value of daily max temperature	TXn	°C
	Coldest night	Monthly and annual lowest value of daily min temperature	TNn	°C
Other index	Warm spell duration index	Annual count when at least six consecutive days of max temperature > 90th percentile	WSDI	d
	Growing season length	Annual (1 January to 31 December in Northern Hemisphere, 1 July to 30 June in Southern Hemisphere) count between first span of at least 6 days with TG > 5 °C and first span after 1 July (1 January in SH) of 6 days with TG < 5 °C (where TG is daily mean temperature)	GSL	d
	Diurnal temperature range	Annual mean difference between daily max and min temperature	DTR	°C
Complex index	Extreme temperature range	The difference between TXx and TNn	ETR	°C
	Compound heatwave	Percentage of time when daily max temperature and daily min temperature > 90th percentile	CHW	d
	Compound heatwave and relative humidity	Percentage of time when daily max temperature and daily min temperature > 90th percentile and relative humidity > 20th percentile	CHW-RH20	d

2.3.1. Linear Tendency Estimation Method

The linear tendency estimation method is an analysis of changes in climate factors that show a continuous increase or decrease over a long time series [44]. It uses the tendency rate of a univariate linear regression equation to study the change trend of the climate index, which is calculated as follows:

$$S = ax + b \quad (1)$$

where S is the extreme climate element, x refers to time, a is the slope of the linear fitting curve (which is the interannual tendency rate), and b is the constant term of the linear regression curve. When $a > 0$, the larger a is, the more obvious the upward trend; conversely, when $a < 0$, the smaller a is, the more obvious the downward trend.

2.3.2. Mann–Kendall Test

The Mann–Kendall (M-K) test is a non-parametric test method that is recommended by the World Meteorological Organization and has been widely used. Its advantages stem from its ability to process a variety of complex data and its flexibility to adapt to constantly changing environmental conditions. It is currently widely used in both hydrology and meteorology [45]. Assuming a set of time series x_1, x_2, $x_3 \ldots x_n$, the M-K trend test is calculated as follows:

$$S_k = \sum_{k=1}^{n=1} \sum_{j=k+1}^{n} sgn(x_i - x_j) \tag{2}$$

$$sgn(x_i - x_j) = \begin{cases} 1, & x_i - x_j > 0 \\ 0, & x_i - x_j = 0 \\ -1, & x_i - x_j < 0 \end{cases} \tag{3}$$

$$Var(S_k) = \frac{n \times (n-1)(2n+5)}{18} \tag{4}$$

$$Z = \begin{cases} \frac{S-1}{\sqrt{Var(S)}}, & if\ S > 0 \\ 0 \quad , & if\ S = 0 \\ \frac{S+1}{\sqrt{Var(S)}}, & if\ S < 0 \end{cases} \tag{5}$$

where S_k is the cumulative total number of events in the time series x, i is greater than j, sgn is a sign function, and $Var\ (S_k)$ is the variance of the test statistic S_k. When $Z > 0$, the sequence exhibits an increasing trend, and when $Z < 0$, the sequence exhibits a downward trend. At the given alpha confidence level, if $|Z| < 1.96$, the index shows an insignificant trend of change; if $1.96 \leq |Z| < 2.56$, it shows a significant trend of change (0.05 significance level); and if $2.56 \leq |Z|$, it shows a highly significant trend of change (0.01 significance level).

2.3.3. Pearson Correlation Coefficient

Correlation analysis refers to the analysis of two or more variable elements with correlations to measure the degree of correlation between the two factors. This study used the Pearson correlation coefficient, which is widely used in the field of data analysis, to measure the linear relationship between atmospheric circulation and different extreme temperature indices [46]. The Pearson correlation coefficient can intuitively measure the strength and direction of the linear relationship between different variables, and its formula is as follows:

$$r_{ij} = \frac{\sum_{n=1}^{k} (x_{in} - \overline{x_i})(x_{jn} - \overline{x_j})}{\sqrt{\sum_{n=1}^{k} (x_{in} - \overline{x_i})^2 \sum_{n=1}^{k} (x_{jn} - \overline{y_i})^2}} \tag{6}$$

where k is the length of the sequence of the study time; n is the year; $\overline{x_i}$ is the sample mean of variable x_i; $\overline{x_j}$ is the sample mean of variable x_j; r_{ij} is the correlation coefficient, and its value range is $(-1, 1)$. r_{ij} greater than 0 indicates a positive correlation, r_{ij} less than 0 indicates a negative correlation, and r_{ij} equal to 0 indicates zero correlation. A greater absolute value of r_{ij} indicates a higher degree of correlation.

3. Results and Analysis

3.1. Temporal and Spatial Variation Characteristics of Extreme Temperature Index

3.1.1. Temporal Trends in Extreme Temperature Index

The characteristics of the extreme temperature index changes on the Chinese mainland from 1961 to 2021 are shown in Figure 2. From the relative index trend chart (Figure 2a–d), the cold indices TX10P and TN10P increased at a rate of 0.17d/(10a) and 0.15 d/(10a), respectively, with an average annual occurrence of approximately 31d and 30d. The warm indices TX90P and TN90P increased at a rate of 1.39d/(10a) and 2.47d/(10a), respectively, with average annual occurrence days of approximately 11d and 13d. The growth rate of the warm indices was much faster than that of the cold indices, and the warming rate at

night was almost twice as high as during the day. From the absolute index trend chart (Figure 2e–h), FD0 and ID0 showed decreasing trends, with interannual tendency rates of −2.91d/(10a) and −0.98d/(10a), respectively. The average number of days with a temperature increase over the years was about 79d and 23d, while SU25 and TR20 showed a significant upward trend, increasing at rates of 3.02d/(10a) and 2.72d/(10a), respectively. The average number of days with a temperature increase over the years was about 131d and 65d, indicating that the number of days with a temperature increase has been gradually increasing across the country, with the largest increase in summer. From the trend chart of the extreme value index (Figure 2i–l), TXx, TNx, TXn, and TNn all showed an upward trend, with interannual trend rates of 0.17 °C/(10a), 0.23 °C/(10a), 0.23 °C/(10a), and 0.43 °C/(10a), respectively. The high temperature index had average annual temperatures of 35.8 °C and 24.6 °C, and the low temperature index had average annual temperatures of −3.1 °C and −12.1 °C, indicating that the maximum and minimum temperatures in the country are both increasing year by year, and the minimum value of the lowest temperature had the largest growth rate. From the other index trend charts (Figure 2m–o), WSDI showed an insignificant downward trend with an interannual tilt rate of −0.03d/(10a), and GSL showed a significant upward trend with an interannual tilt rate of 2.6d/(10a), indicating that the growing season length increased with the increase in temperature across the country, with DTR showing a downward trend with an interannual tilt rate of −0.08 °C/(10a), indicating that the difference between the maximum and minimum daily temperatures is decreasing. Overall, the cold indices FD0 and ID0 showed a significant downward trend, which may be due to the increases in TX10P, TN10P, TNx, and TNn leading to a decrease in the number of freezing and frost days. The WSDI and DTR showed a slow downward trend, and all other indices showed an increasing trend, indicating that the occurrence of extreme cold events gradually decreased over the past 60 years. Overall temperatures continued to increase, with the daily increase at low temperatures being greater than that at high temperatures.

3.1.2. Spatial Variation Trend in the Extreme Temperature Index

The spatial variation characteristics of the extreme temperature indices in China from 1961 to 2021 were analyzed using the M-K trend test method (as shown in Figure 3). From the spatial distribution map of the relative indices, the percentage of sites with decreasing indices was <1%. The TX10P distribution map shows that 48.74% of the sites had a highly significant upward trend, mainly concentrated in the eastern part of the MTA, southwestern part of the NSH region, and MTH region. The sites with an insignificant trend were concentrated in the south–central part of the WTSH region and north–central part of the NSH region, and the sites with a significant upward trend were distributed in the central parts of the MTSA, MTSH, and NSH region. The TN10P chart shows that 85.36% of the sites had no significant trend, while the sites with extremely significant and significant upward trends were distributed in the southern part of the MTH region and the other seven zones, respectively. The TX90P chart shows that 43.69% of the sites had no significant trends, mainly distributed in the western part of the MTA region, southwestern part of the MTSH region, south–central part of the WTSH region, and north–central part of the NSH region. The sites with a very significant upward trend were mainly concentrated at the NSH edge and in the MTH region, while the sites with a significant upward trend were mainly distributed in the middle parts of the MTS, WTSH, and NSH regions. The TN90P chart shows that 71.76% of the sites showed a significant upward trend, while the sites with an insignificant trend were distributed in the southern part of the WTSH region and northern part of the NSH region. The number of sites with a significant upward trend was half that of sites with an insignificant trend, mainly concentrated in the central areas of the WTSH and NSH regions. From the spatial distribution diagram of the absolute index, the cold indices FD0 and ID0 mainly showed a significant downward trend and an insignificant trend, while the warm indices SU25 and TR20 mainly showed a significant upward trend. As shown in Figure 3e, 79.65% of the sites showed a significant downward

trend, mainly distributed in the other six regions except the MTH region, and the sites with an insignificant trend were concentrated in the MTH region. The ID0 chart shows that 61.11% of the sites showed no significant trend and were mainly distributed in the MTA, NSH, and MTH regions. The sites with a significant downward trend were mainly concentrated in the western part of the MTSA region, eastern and western parts of the WTSH region, and eastern part of the SU25 chart; 69.39% of the sites showed a significant upward trend, mainly distributed in the north and south of the WTSH, NSH, and MTH regions. The sites with an insignificant trend were distributed in the central areas of the WTSH, NSH, and MTH regions and east of the PTSA region. The sites with a significant upward trend were distributed throughout the MTSH and WTSH region. According to the TR20 chart, 71.17% of the sites showed a highly significant upward trend, mainly distributed in the eastern part of the WTSH region, central and eastern parts of the NSH region, and MTH region, whereas sites with no significant trends were mainly concentrated in the western part of the NSH region and central and eastern parts of the PTSA region. From the spatial distribution map of the extreme value index, the proportion of sites with a downward trend for each index was the same as that of the relative index, while the growth trends of TXx and TXn were not significant, and TNx and TNn showed highly significant upward trends. As shown by the TXx distribution, 57.02% of the sites showed no significant trend and were mainly distributed in the central areas of the MTSA, MTSH, WTSH, and NSH regions. The sites with a significant upward trend were mainly distributed at the NSH edge and in the MTH region, and the sites with a significant upward trend were distributed in the south of the MTSH and NSH regions. As shown in the TNx chart, 64.91% of the sites showed a significant upward trend, mainly distributed in the PTAS, WTSH, NSH, and MTH regions; the sites with an insignificant trend were mainly distributed in the south–central part of the WTSH region and the north–central part of the NSH region, while the sites with a significant upward trend were scattered in the MTSH, WTSH, and NSH regions. As shown in the TXn chart, 73.78% of the sites had an insignificant trend, mainly distributed in the southern part of the MTSH region, eastern part of the WTSH region, southern part of the NSH region, and MTSA and MTH regions. The sites with significant upward trends were mainly concentrated in the NSH region, and the sites with extremely significant upward trends were mainly distributed at the intersection of the PTSA, NSH, and WTSH regions. As shown in the TNn chart, 53.87% of the sites showed a highly significant upward trend, mainly distributed in the eastern part of the WTSH region and southern parts of the NSH and MTH regions. The sites with an insignificant trend were mainly distributed in the central and western parts of the WTSH region and northeastern part of the NSH region, while the sites with a significant upward trend were distributed throughout the WTSH and NSH regions. From the spatial distribution maps of other indices, WSDI showed an overall significant trend, with sites accounting for as much as 94.83%; the sites with a significant upward trend of GSL were the highest, mainly distributed in the eastern and western parts of the MTSA region, the southwestern part of the MTSH region, and the WTSH region. The sites with an insignificant trend were mainly distributed in the central and southern parts of the NSH and MTH regions. The sites with a significant downward trend in DTR accounted for 59.24%, mainly distributed in the entire MTSH region and the eastern part of the WTSH region, and sites with an insignificant trend were mainly concentrated in the central part of the NSH region.

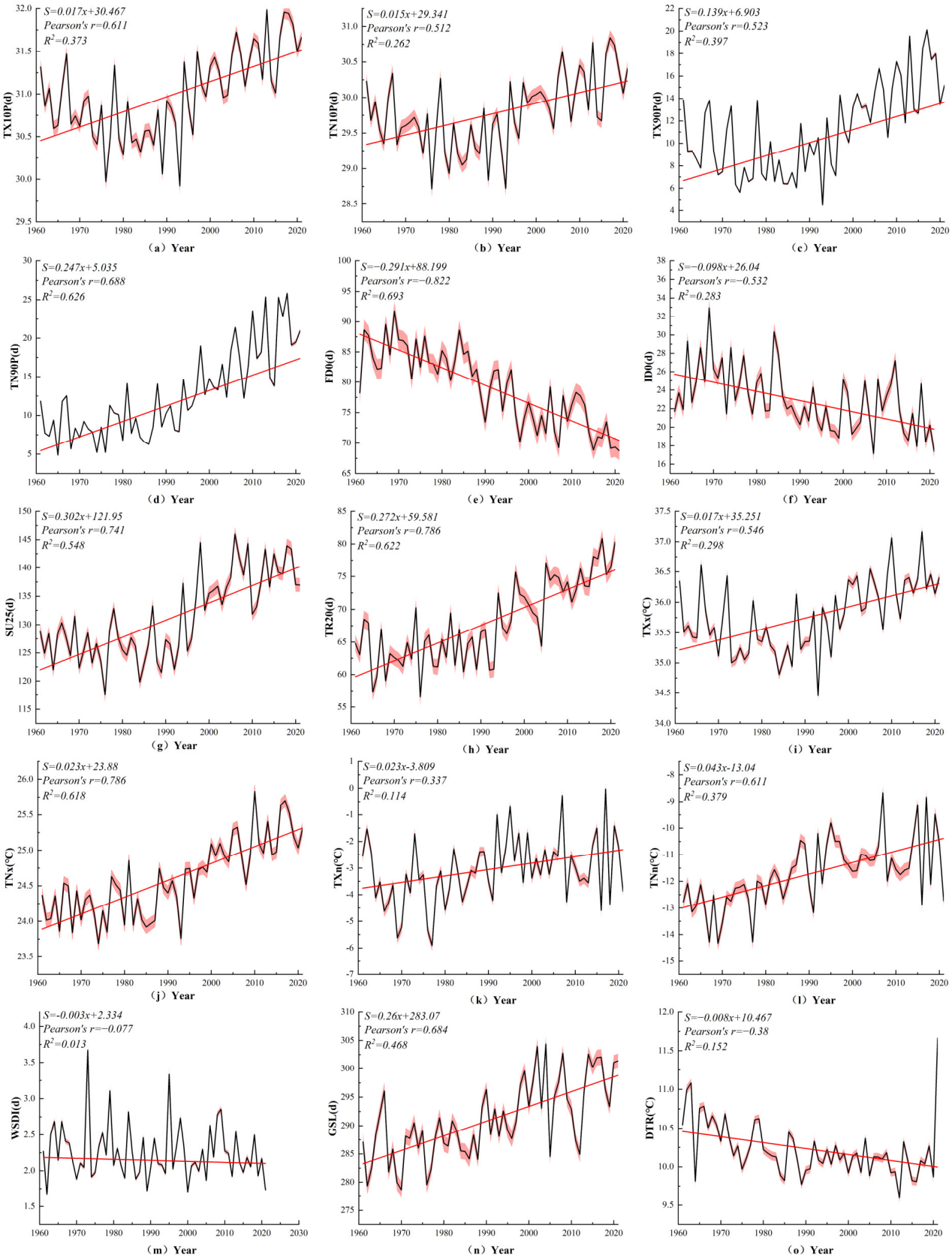

Figure 2. Time variation trend in the extreme temperature index on the Chinese mainland. [(**a**) TX10P; (**b**) TN10P; (**c**) TX90P; (**d**) TN90P; (**e**) FD0; (**f**) ID0; (**g**) SU25; (**h**) TR20; (**i**) TXx; (**j**) TNx; (**k**) TXn; (**l**) TNn; (**m**) WSDI; (**n**) GSL; (**o**) DTR]. (The red area in the figure shows the error bands of the values).

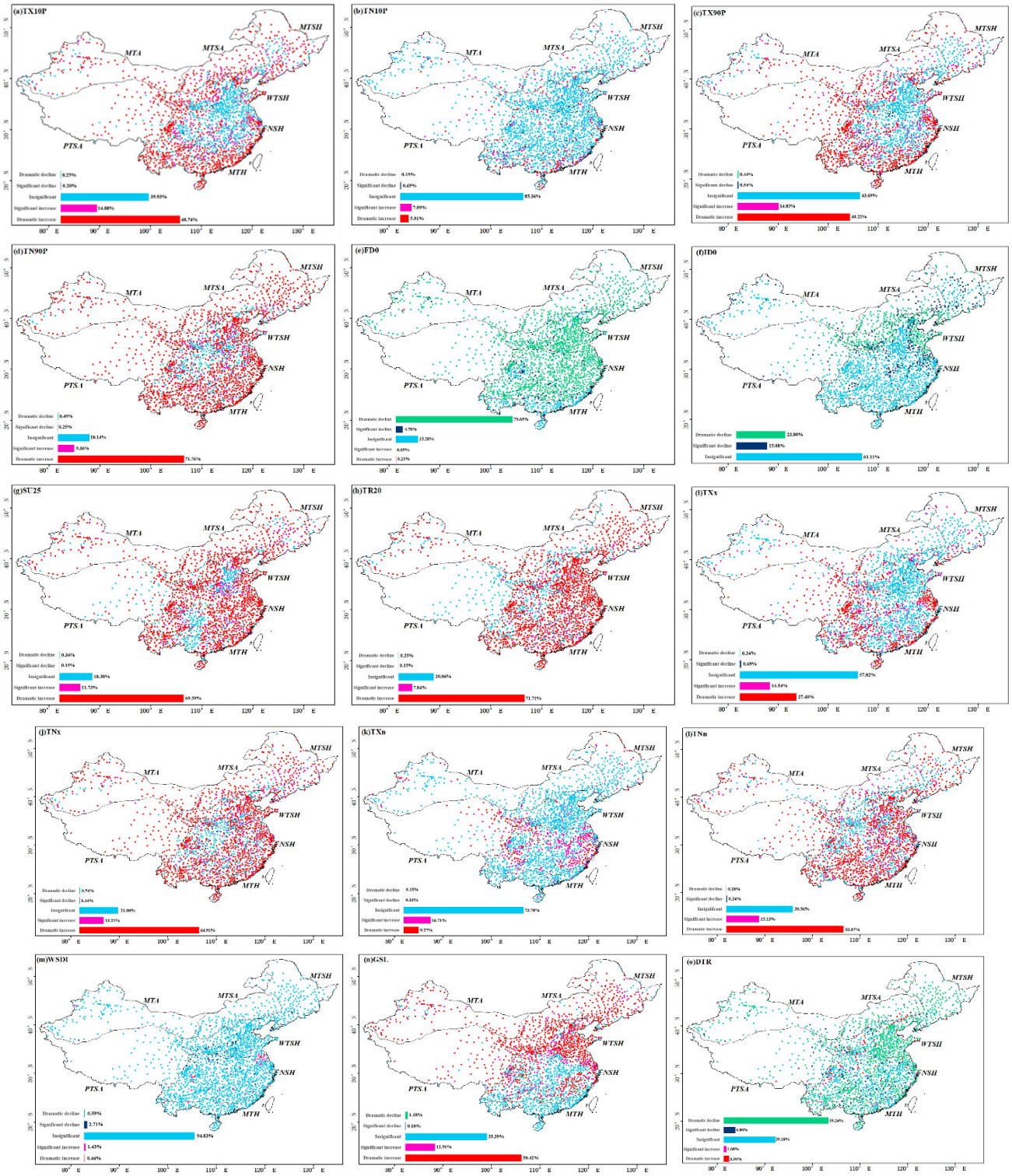

Figure 3. Spatial variation trend in the extreme temperature index on the Chinese mainland. [(**a**) TX10P; (**b**) TN10P; (**c**) TX90P; (**d**) TN90P; (**e**) FD0; (**f**) ID0; (**g**) SU25; (**h**) TR20; (**i**) TXx; (**j**) TNx; (**k**) TXn; (**l**) TNn; (**m**) WSDI; (**n**) GSL; (**o**) DTR]. (Red indicates a dramatic increase, pink indicates a significant increase, light blue indicates insignificant, dark blue indicates a significant decline, and green indicates a dramatic decline).

Overall, TX10P, TN90P, SU25, TR20, TNx, TNn, and GSL showed a significant increasing trend during the study period, and these changes were concentrated in the WTSH, NSH, and MTH regions, indicating that the frequency and intensity of extreme temperature

events in these regions are increasing. At the same time, TN10P, TX90P, ID0, TXx, TXn, and WSDI showed no significant trends, with the proportion of stations ranging from 57% to 95%, indicating that there has been no significant change in the performance of extreme-temperature events in each region. FD0 and DTR mainly showed significant decreases, which may indicate that certain regions are experiencing sustained warming. The trend in the temperature index growth varies in different regions and is closely related to factors such as geographical location, altitude, and climate conditions in each region. These results demonstrate the spatial distribution characteristics of extreme temperature indices in different climatic regions of the Chinese mainland and reveal their complex trends and features. The trend in the extreme temperature index shows high consistency in both time and space, indicating that although climate change varies in different regions, there are still significant similarities in the temporal and spatial changes in extreme climate events at the macro level.

3.2. Spatiotemporal Variation Characteristics of the Extreme Composite Temperature Index

3.2.1. Time Trend in the Extreme Composite Temperature Index

The trend in the extreme composite temperature index proposed in this study over the past 61 years is shown in Figure 4. According to Figure 4a, the multi-year mean value of ETR fluctuated between 45 and 51 °C and decreased at a rate of 0.26 °C/(10a), indicating that the temperature difference between day and night has been gradually decreasing. Although both TXx and TNn showed a continuous upward trend over the past 60 years, the rate of temperature increase at night was approximately 2.5 times that during the day, and this uneven heating rate is also directly responsible for the reduction in ETR. Figure 4b shows that the variation amplitude of CHW was relatively stable before 2000, and the occurrence of composite high temperature remained for approximately 3 days, but the growth rate accelerated significantly after this period. This is consistent with the temporal trend of TX90P and TN90P. Specifically, the frequency of CHW increased year by year at a rate of 1.02d/(10a). Figure 4c shows the trend of CHW-RH20, which had a significantly lower growth rate than the first two composite indices. The average number of occurrence days over the years was 0.5d, and the growth rate was 0.1 days/(10a). This lower growth rate may be due to the addition of screening conditions, resulting in a trend of growth in this composite index that is not as significant as that for the other indices. However, although the growth trend of CHW-RH20 was slightly less than that of other extreme composite temperature indices, its impact on human life and the ecological environment was much greater than that of other composite high-temperature events. Overall, the growth trend of the extreme composite temperature index was significantly lower than that of the conventional temperature index. This suggests that although the frequency and intensity of composite high-temperature events have increased, their growth rate is not as fast as that of single extreme temperatures. Therefore, it is particularly important to consider changes in these composite temperature indices when assessing the impact of a changing climate environment on human society.

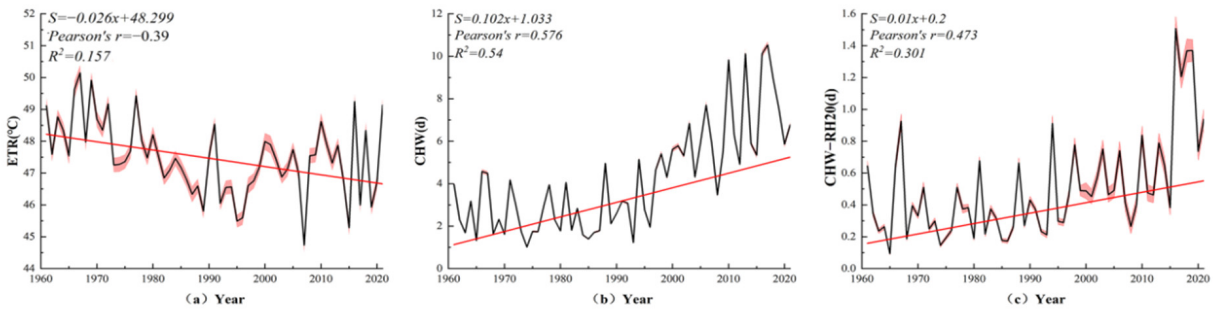

Figure 4. Time variation trend in the extreme composite temperature index on the Chinese mainland. [(**a**) ETR; (**b**) CHW; (**c**) CHW−RH20]. (The red area in the figure shows the error bands of the values).

3.2.2. Spatial Variation Trend in the Extreme Composite Temperature Index

Figure 5 shows the spatial trends in the extreme composite temperature indices. From the ETR distribution map, it can be seen that 59.73% of the sites had insignificant increasing trends, and these sites were mainly concentrated in the western part of the WTSH region and the entirety of the NSH region. Relatively speaking, the sites with a significant downward trend were mainly concentrated in the central areas of the WTSH, NSH, and MTH regions, while the sites with a significant downward trend were distributed in the MTSH, WTSH, and NSH regions; moreover, the proportion of sites with significant upward and extremely significant upward trends was less than 2%, and these sites were mainly located in the northwest of the NSH region. The CHW distribution map shows that 55.54% of the sites showed a significant upward trend, and these sites were mainly located in the MTSA, MTH, and PTSA regions, as well as the edge zones of the WTSH and NSH regions. The sites with a significant upward trend were concentrated in the central areas of the MTSH, WTSH, and NSH regions, while the sites with an insignificant trend are mainly located in the south of the WTSH region and north of the NSH region. The percentage of sites with significant downward and extremely significant downward trends was less than 0.5%. The distribution map of CHW-RH20 shows that 87.93% of the sites had no obvious change trend, with 6.31% and 4.9% of the sites showing extremely significant upward and significant upward trends, respectively. They were mainly distributed in the central and peripheral areas of the NSH region, as well as at the edges of the WTSH and MTH regions. The proportion of sites showing extremely significant downward and significant downward trends was <1%. Overall, the spatial variation trends in the three extreme composite temperature indices were highly consistent with the temporal variation trends, while the spatial values of ETR and CHW were highly consistent with the conventional extreme temperature indices; the increasing trend of CHW-RH20 was not significant at the national level, probably due to the increase in constraint variables.

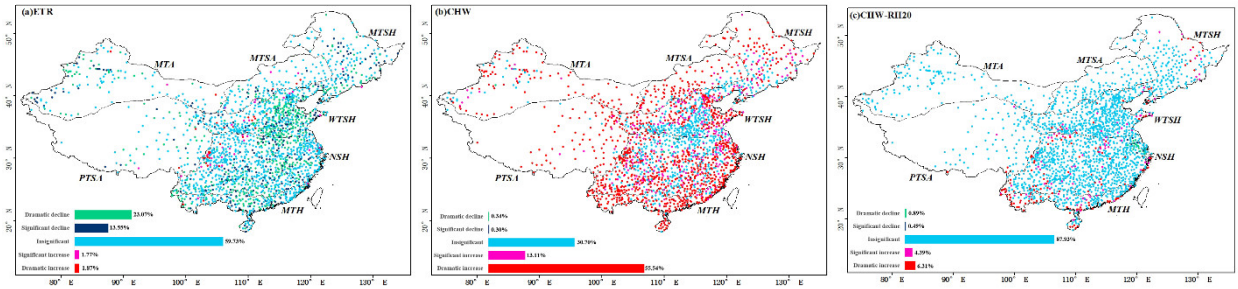

Figure 5. Spatial change trend in the extreme composite climate index on the Chinese mainland. [(**a**) ETR; (**b**) CHW; (**c**) CHW−RH20]. (Red indicates a dramatic increase, pink indicates a significant increase, light blue indicates insignificant, dark blue indicates a significant decline, and green indicates a dramatic decline).

3.3. Correlation Between Extreme Temperature Index and Atmospheric Circulation Index

Atmospheric circulation is an important factor that affects extreme climate events on a large scale. To further expand the analysis perspective of extreme temperature indices, this study divided the entire research area into seven different climate regions for elaboration. The relationships between Arctic Oscillation (AO), Atlantic Multiannual Oscillation (AMO), El Niño–Southern Oscillation (ENSO), North Atlantic Oscillation (NAO), Pacific Decadal Oscillation (PDO), and extreme climate indices from 1961 to 2021 were selected for Pearson correlation analysis. The specific results are shown in Figure 6, which illustrates the complex relationship more clearly. The fan colors were used to visually present the correlations between different atmospheric circulation indices and climate indices in various climate zones. Positive correlations are shown in red, negative correlations are shown in blue, and the strength of each correlation is reflected by the depth of the color: the stronger the correlation (i.e., the closer to −1 or 1), the darker the color.

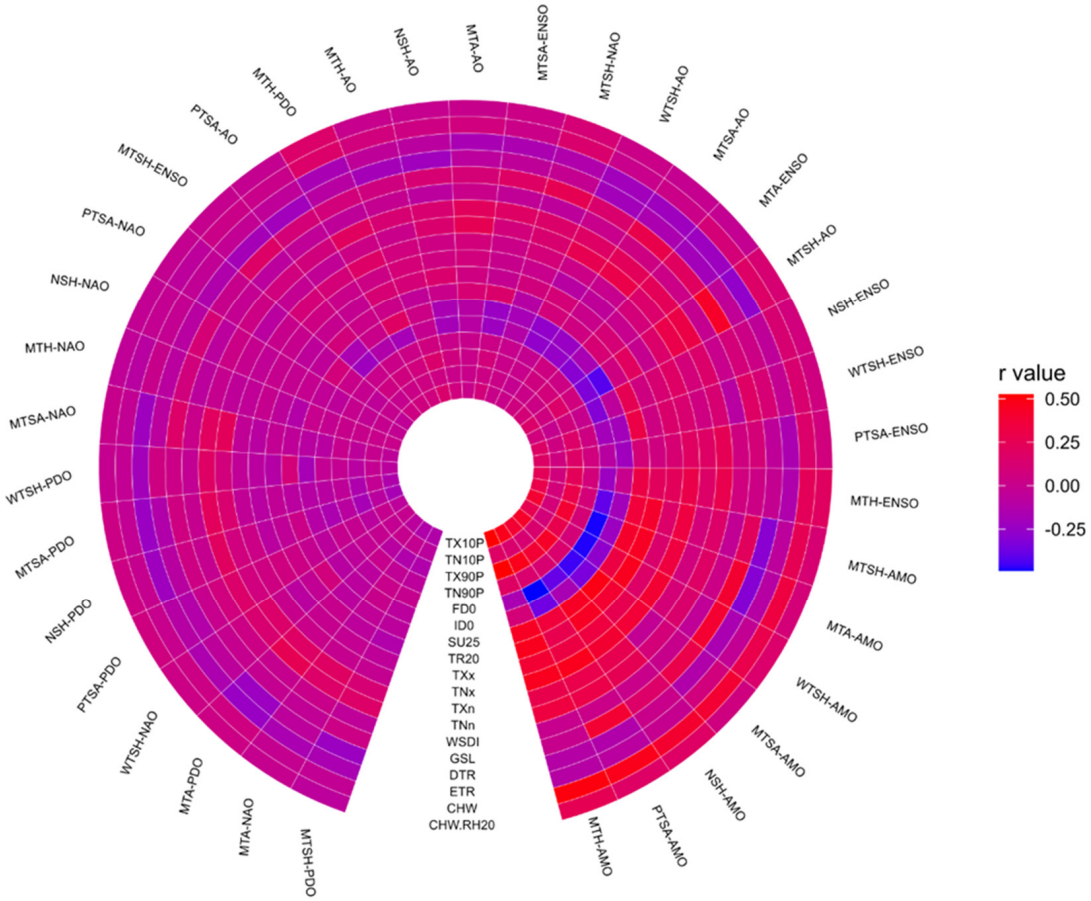

Figure 6. Correlation coefficients between extreme climate index and atmospheric circulation index in seven climate regions during 1961–2021.

From the analysis of Figure 6, it can be seen that in the MTA region, there was a negative correlation between AO and AMO with the extreme temperature indices FD0, ID0, DTR, and ETR. The correlation coefficient of FD0 reached −0.48, indicating a strong negative correlation. Meanwhile, TR20 had the highest correlation of 0.44, indicating that extreme high-temperature events were more significant and extreme low-temperature events were reduced under the warm phase of AO and AMO. In the negative correlation between the El Niño phenomenon and these factors, the correlation coefficient of the newly added TXx was −0.001, indicating that the warm phase of ENSO has some influence on extreme high-temperature events, but its influence is relatively small. The NAO was positively correlated with FD0, ID0, TXx, TNn, and the duration of extreme weather, while it showed a negative correlation trend with other temperature indices, and the correlation coefficient showed a clear opposing relationship. In the positive correlations between PDO and TNx, TXn, TNn, CHW, and CHW-RH20, TNn had the highest value of 0.25, while in the negative correlations with other indices, ETR had the highest correlation coefficient of −0.24.

In the PSTA region, AO was negatively correlated with FD0, TR20, TXn, WSDI, DTR, ETR, and CHW-RH20 and positively correlated with other extreme temperature indices, especially DTR, with a correlation coefficient of −0.2, indicating a decreasing trend in daily temperature differences as AO increased. The negative correlations between AMO and ENSO with FD0, ID0, ETR, and DTR were significant, with AMO having the highest negative correlation coefficient with FD0, reaching −0.49, while ENSO's impact was slightly inferior. The correlation coefficients of TX10P, TX90P, TNx, and CHW were all above 0.4, indicating a strong positive correlation between these indices and AMO. NAO showed positive correlations with FD0, ID0, TNx, TNn, and GSL, while showing negative

correlations with other extreme temperature indices. The positive correlations between PDO and TR20, TXx, TNx, TXn, TNn, WSDI, and CHW-RH20 were significant, while the negative correlations with other indices were also prominent.

In the MTSA region, AO was negatively correlated with FD0, ID0, TXx, TNx, DTR, ETR, and CHW-RH20, while it was positively correlated with other temperature indices. AMO was negatively correlated with FD0, ID0, TXn, and DTR, with a correlation coefficient of −0.46 for FD0. However, among the positive correlations with other temperature indices, the correlation coefficients for TX10P, TX90P, SU25, and TR20 were all above 0.4. CHW-RH20 was excluded from the negative correlation between ENSO and these factors. The positive correlations between NAO and TXn, TNn, WSDI, GSL, and CHW-RH20 were more pronounced, while the index positively correlated with POD was less than the WSDI index in NAO.

In the MTSH region, among the negative correlations between AO and FD0, ID0, TXx, WSDI, DTR, and ETR, ID0 had the highest value of −0.42, while among the positive correlations with other indices, GSL had the highest value of 0.42. This indicates that with the increase in AO, the number of freezing days decreases continuously, while the length of the growing season continues to increase. Among the negative correlations between AMO and these factors, TXx was excluded, while FD0 showed a strong negative correlation with a correlation coefficient of −0.4. Among the positive correlations with other factors, the correlation coefficients of SU25 and TR20 were above 0.35, indicating that AMO has a strong impact on extreme thermal events. ENSO was negatively correlated with TN10P, FD0, ID0, TR20, TXx, WSDI, DTR, ETR, and CHW-RH20, while it was positively correlated with other factors. NAO was negatively correlated with TN90P, FD0, ID0, SU25, WSDI, DTR, and ETR, and positively correlated with other factors. PDO was only positively correlated with TXn and TNn, indicating that as PDO increases, the minimum values of the daily maximum and minimum temperatures gradually increase.

In the WTSH region, AO was negatively correlated with TN10P, TN90P, FD0, ID0, TXx, DTR, and ETR, and positively correlated with other temperature indices. In the negative correlations between AMO and FD0, ID0, WSDI, DTR, and ETR, FD0 had the highest value of −0.48, while in the positive correlations with other factors, TR20 had the highest value of 0.46. This indicates that as AMO increases, the overall temperature continues to rise. Compared with factors that had a negative correlation with ENSO, AMO had less DTR, indicating that the difference in tomorrow's temperature continues to increase. NAO was positively correlated with SU25, TNx, TXn, TNn, WSDI, CHW, and CHW-RH20 and negatively correlated with other factors. PDO was positively correlated with SU25, TXn, TNn, GSL, and DTR, and negatively correlated with other factors.

In the NSH region, AO was negatively correlated with FD0, ID0, WSDI, DTR, ETR, and CHW-RH20 and positively correlated with other factors. Compared with factors negatively correlated with AMO, AO reduced WSDI, DTR, and CHW-RH20, with the highest value for FD0 being −0.39. Among other positively correlated factors, the correlation coefficients of SU25, TR20, and CHW were all above 0.4. ENSO was negatively correlated with TN10P, TN90P, FD0, ID0, and ETR, and positively correlated with other factors. NAO was only positively correlated with TNn and GSL, and compared with the factors positively correlated with PDO, NAO increased SU25, TNx, TXn, and CHW-RH20.

In the MTH region, AO was negatively correlated with FD0, SU25, WSDI, GSL, DTR, ETR, and CHW-RH20, and positively correlated with other factors. The factors negatively correlated with AMO reduce SU25 and increase GSL compared to AO. The correlations among the positive correlation factors were relatively strong, with TX10P, TX90P, and CHW all having correlation coefficients of over 0.5. ENSO was negatively correlated with FD0, ID0, DTR, and ETR, and positively correlated with other extreme temperature indices. NAO was positively correlated with TX10P, TN10P, TX90P, TN90P, GSL, and ETR. PDO was negatively correlated with FD0, WSDI, DTR, and ETR and positively correlated with other factors.

In summary, FD0, ID0, DTR, and ETR were generally negatively correlated with various atmospheric circulation indices throughout the study area, which indicates a gradual decrease in the occurrence of extreme low-temperature events. In the MTH region, due to its abundant uneven precipitation and high temperature, the correlations between the atmospheric circulation index and extreme temperature index were particularly evident, showing more significant temperature characteristics compared with other regions. Specifically, AO, AMO, and ENSO were mainly positively correlated with extreme climate indices, with AMO having the highest correlation coefficient. This is because the warm phase of the global atmosphere usually suppresses the southward movement of cold air, leading to frequent extreme heat events. On the contrary, the relationship between NAO, PDO, and the extreme climate index showed the opposite trend. When NAO is in the negative phase, the eastward extension of the North Atlantic jet stream strengthens, leading to anticyclonic circulation over China and insufficient water vapor transport, thereby reducing the frequency of extreme heat events. The negative phase of PDO usually leads to a decrease in sea surface temperature in the Pacific region, affecting the climate patterns of surrounding areas and resulting in a decrease in the frequency of extreme heat events.

4. Discussion

The World Meteorological Organization recently issued a press release officially confirming 2023 as the hottest year on record. Climate anomalies have also triggered many meteorological disasters around the world, including heatwaves, droughts, torrential rains and floods, typhoons, and forest wildfires [47]. The occurrence of extreme weather in China has increased in frequency in recent years, affecting a wide range of areas, intensifying, and setting historical records. There has been an increase in the number of sudden events without warning signs. In the early summer of 2023, North China and Huang Huai suffered five consecutive rounds of heatwaves, with a total of 22 national meteorological stations breaking historical records for the highest temperatures. Specifically, over 70% of areas in Beijing and Tianjin experienced temperatures above 40 °C. Extreme weather undoubtedly exacerbated living difficulties and economic losses among the people [48]. In December of the same year, China experienced the strongest cold wave on record during the same period, with many areas setting new records for low temperatures and snow accumulation. Global warming will affect the atmospheric circulation pattern, and through the interaction of ocean and land meteorology, it will affect the occurrence patterns of extreme weather events in different regions. From a long-term trend perspective, the frequency of extreme high-temperature events is indeed increasing, while the frequency of extreme low-temperature events has decreased, but their intensity has not weakened. This indicates that the intensity and impact of extreme weather are highly volatile and severe in the context of warming.

In order to be able to better cope with and mitigate the challenges posed by extreme temperature events, this study closely examined the changes in 15 commonly used extreme temperature indices and 3 extreme composite temperature indices using data from a total of 2029 meteorological stations in China over the period 1961–2021. This study explored the temporal and spatial trends in these indices and revealed their complex internal mechanisms through correlation analyses with atmospheric circulation. The research results show that the frequency and intensity of extreme high-temperature events have increased significantly over the past 60 years, while the number of extreme low-temperature events has decreased. This finding is consistent with the conclusions of most domestic studies, that is, that the intensity, frequency, and duration of extreme high-temperature events have all increased significantly [49]. The trend in the extreme composite temperature index is similar to that in the extreme temperature index, but the magnitude of the change is relatively small. Overall, the temporal and spatial variations in extreme temperature indices show a high degree of consistency, suggesting broad commonality in the variability of extreme-temperature events. It has been pointed out that the number of warm nights has significantly increased globally over the past 70 years, while the number of frost and freez-

ing days has decreased; the daily difference in temperature has also decreased significantly, and the variability in the rate of regional change is significant [50]. Based on the data after 1961, this study found that FD0 and ID0 showed a significant decreasing trend on a national scale, while DTR showed a slow decreasing trend, which is in strong agreement with the results of previous studies. Although some scholars have pointed out that the increase in extreme low temperatures in China is significantly larger than that in extreme high temperatures, the study of a single variable has been insufficient to meet the complex needs of climate change mitigation. Therefore, this paper proposes a new extreme composite temperature index, with the finding that ETR shows a decreasing trend in both time and space, mainly due to the fact that the increase in temperature at night is greater than that during the day. Zhang Jiayi et al. analyzed the variation in linear trends in high-temperature heatwaves in China using data from 1960 to 2018, observing that the numbers of high-temperature days and heatwaves significantly increased only in the South China region and Northwest China region, while the trends in the North China region and Northeast China region were insignificant, and the national average numbers of high-temperature days and heatwaves significantly increased [51]. In this study, the performances of extreme heat indices such as TX90P, TXx, SU25, and CHW were found to be different, with TX90P and TXx showing insignificant trends nationwide but highly significant increasing trends in the MTH region and at the NSH fringe, and SU25 and CHW showing highly significant increasing trends nationwide but insignificant trends in the NSH region and at the WTSH fringe. The reason for this difference may lie in the different definitions of extreme temperature indices and high temperatures, as well as the accelerated rate of extreme climate change in recent years. Cao Qing et al. used linear fitting, R/S analysis, and other methods to analyze the trend, spatiality, persistence, and mean cycle length of extreme climatic elements in China for 58a, and the results showed the following: The temperature extremes, as well as the frequency and persistence of extreme high-temperature events, showed upward trends, while the number of low-temperature events showed a decreasing trend, with an overall warming trend observed across China [52]. Spatially, the extreme temperature indices in the plateau mountainous areas showed high variation. These results slightly differ from the results of this study, in which the temperature extremes during the daytime mainly showed an insignificant trend, and those at night mainly showed a significant upward trend, indicating that the increase in high-temperature extremes has recently slowed down, but low-temperature extremes are still growing continuously.

With the intensification of global warming, hotter weather will evolve into compound extreme weather, which more severely impacts socio-economic and environmental aspects compared to single extreme events. Chen Yang et al. used meteorological data from 756 stations between 1961 and 2015 to analyze the frequency, duration, and intensity of independent hot days, independent hot nights, and composite events in summer in China [53]. Their research results indicated that, except for in the central and eastern regions of China, the frequency, duration, and intensity of composite extreme weather events are higher, while the frequency of independent hot weather events in the central and eastern to northeastern regions of China shows a significant downward trend. The linear trend of nighttime hot events is similar to that of composite events. The extreme composite temperature indices CHW and CHW-RH20 proposed in this article cover daytime high temperatures, nighttime high temperatures, and relative humidity. Both of these indices showed an upward trend over time, but their growth rate was lower than that of the conventional extreme temperature index. In terms of spatial distribution, the CHW index showed a significant increasing trend, while the change trend of the CHW-RH20 index was not significant. The reasons for these different research results may include the introduction of relative humidity variables into the composite index, which has not been fully explored in previous studies. In addition, research results heavily rely on the choice of start and end years [54].

The occurrence of extreme weather is influenced by various factors, including altitude, topography, climate environment, human activities, and atmospheric circulation.

Numerous studies have shown a correlation between the atmospheric circulation index and extreme climate index [55–57]. Wu et al. explored the relationship between extreme climate change and atmospheric circulation based on data from 41 meteorological stations in the Haihe River Basin from 1961 to 2020, and found that the AO has a strong influence, being generally positively related to the extreme warmth index and negatively related to the extreme coolness index, with multiple resonant cycles between the AO and extreme climate index in the Haihe River Basin [58]. Su et al. studied the influence of the seasonal average maximum temperature and atmospheric circulation in China from 1950 to 2019, finding that the Pacific decadal oscillation was significantly negatively correlated with summer high temperatures [59]. The North Atlantic oscillation had a significant positive influence on high-temperature changes in summer, autumn, and winter, while the Arctic oscillation had a significant influence on high temperatures in all seasons. The El Niño–Southern Oscillation had significant positive or negative effects on short-term changes in high temperatures in spring and summer depending on the year of its cause. Gao et al. explored the relationship between changes in summer high-temperature activity in China and the El Niño phenomenon and found that the high-temperature weather during El Niño in the eastern and central Pacific presents different spatial patterns [60]. Among them, the westward and northward movement of anticyclones in the upper troposphere of the western North Pacific coincides with the anomalous subsidence in southern China. El Niño events usually increase heatwave activity in southern China. Liu et al. used daily maximum temperature data from 654 observation stations in China and global reanalysis data to analyze decadal changes in the association between subtropical high pressure and heatwaves in the western Pacific from 1959 to 2016 [61]. They found that the correlation coefficient between subtropical high-intensity and heatwave days during the positive phase of PDO was 0.65, while it was only 0.12 during the negative phase of PDO. Compared with the negative phase of PDO, the warming of the Indian Ocean in the summer of ENSO attenuation years is stronger in the positive phase of PDO, which further promotes the strengthening of anticyclones in the northwest Pacific and is conducive to more heatwaves in eastern China. On more decadal or long-term scales, high-temperature events are believed to be related to Atlantic decadal oscillation [62]. This study examined the correlation between the extreme temperature index and atmospheric circulation indexes at different scales, finding that there is a generally negative correlation between FD0, ID0, DTR, and ETR and atmospheric circulation indexes throughout the region. Due to the unique geographical location and climate characteristics of the MTH region, its correlation is more significant than that in other areas. Specifically, AO, AMO, and ENSO are positively correlated with the extreme temperature index, with AMO having the highest correlation coefficient, while NAO and PDO are negatively correlated with the extreme temperature index.

Extreme climate change is a continuous and complex process, and the limited number of extreme temperature indices analyzed in this study may have resulted in an insufficient assessment of extreme temperatures in the overall region. Extreme temperature changes in the region may lead to changes in the regional radiation energy balance and atmospheric circulation patterns, thereby affecting the regional climate. The research method in this study was mainly based on statistical methods, and its results and conclusions need to be combined with an analysis of physical mechanisms to be more convincing. In addition, numerous studies have pointed out that urbanization, carbon emissions, and heat island effects also have a huge impact on extreme climate events, which will become a new hotspot in future research.

5. Conclusions

This paper presented a comprehensive spatial and temporal analysis of fifteen conventional extreme temperature indices and three extreme composite temperature indices for seven climatic regions on the Chinese mainland. By using various statistical analyses and combining several large-scale climate indices, the evolution of these extreme climate

indices was assessed, and their influencing factors were clarified. The main conclusions are as follows:

(1) In terms of extreme temperature indices, the cold indices FD0 and ID0 showed a significant downward trend, while the WSDI and DTR showed a slow downward trend over time. Other indices generally showed an increasing trend. In the past 60 years, the frequency of extreme low-temperature events has gradually decreased, while the frequency of high-temperature events has continued to increase, with the increase on warm nights significantly outpacing that on warm days. From a spatial distribution perspective, TX10P, TN90P, SU25, TR20, TNx, TNn, and GSL mainly showed a significant increasing trend nationwide, especially concentrated in areas such as the WTSH, NSH, and MTH regions. Relatively speaking, TN10P, TX90P, ID0, TXx, and WSDI were not significant in each region, while FD0 and DTR each showed a significant downward trend, which is closely related to the geographical location and climate conditions of each region. Overall, the trends of the extreme temperature index changes in time and space had a high degree of consistency.

(2) In terms of the extreme composite temperature index, ETR showed a downward trend over time, while CHW and CHW-RH20 showed an upward trend. Although the growth trend of the extreme composite temperature index was significantly lower than that of the conventional temperature index, its potential impact is more severe. From a spatial perspective, the trend in ETR and CHW-RH20 changes nationwide was not significant, while the stations that showed a highly significant upward trend were mainly distributed in the WTSH and NSH regions. CHW showed a significant upward trend, mainly distributed across the MTSA, MTH, and PTSA regions, as well as the edge zones of the WTSH and NSH regions. The temporal trends in and spatial distributions of the three extreme composite temperature indices are highly consistent. The spatial distribution of ETR and CHW is highly consistent with the conventional extreme temperature index, while CHW-RH20 may not have a clear upward trend nationwide due to the increase in constraint variables.

(3) In the correlation analysis with atmospheric circulation indexes, FD0, ID0, DTR, and ETR were generally negatively correlated with various atmospheric circulation indexes throughout the study area. However, due to the unique geographical location and climate characteristics of the MTH region, the correlation performance of these indices in this area differed significantly from that in other regions. Specifically, AO, AMO, and ENSO were mainly positively correlated with extreme temperature indices, with AMO having the highest correlation coefficient. This is mainly due to the warm-phase atmospheric circulation, which suppresses the southward movement of cold air, leading to an increase in extreme high-temperature events. Relatively speaking, NAO and PDO exhibited opposite trends to the extreme temperature indices, as being in a negative phase can cause anticyclonic circulation and a decrease in sea surface temperature, thereby reducing the frequency of extreme heat events.

Author Contributions: X.W.: software, validation, writing—original draft preparation, writing—review and editing, and visualization; L.W.: conceptualization, methodology, data curation, project administration, and funding; H.L.: formal analysis, investigation, resources, and supervision. All authors have read and agreed to the published version of the manuscript.

Funding: This research was funded by the Science and Technology Project of Jiangxi Provincial Department of Education (Grant number GJJ180925) and the Development Project of Jiangxi Provincial Department of Science and Technology (Grant number 20212BDH80016).

Institutional Review Board Statement: Not applicable.

Informed Consent Statement: Not applicable.

Data Availability Statement: The dataset supporting the findings of this study are publisher available in Zenodo at https://doi.org/10.5281/zenodo.13841197, with the identifier DOI:10.5281/zenodo.13841197.

Conflicts of Interest: The authors declare no conflicts of interest.

References

1. AghaKouchak, A.; Cheng, L.Y.; Mazdiyasni, O.; Farahmand, A. Global warming and changes in risk of concurrent climate extremes: Insights from the 2014 California drought. *Geophys. Res. Lett.* **2014**, *41*, 8847–8852. [CrossRef]
2. Wang, L. The State Council Issues the "Outline for High-Quality Development of Meteorology (2022–2035)". *China Meteorological News*, 20 May 2022; p. 1.
3. Kuang, S.Y.; Zhou, Z.Y.; Liang, M.C.; Gao, X.; Cao, Y. Sixth IPCC assessment report working group 2 read. *J. Environ. Prot.* **2022**, *50*, 71–75. [CrossRef]
4. Meehl, G.A.; Tebaldi, C. More Intense, More Frequent, and Longer Lasting Heat Waves in the 21st Century. *Science* **2004**, *305*, 994–997. [CrossRef]
5. Perkins-Kirkpatrick, S.E.; Lewis, S.C. Increasing trends in regional heatwaves. *Nat. Commun.* **2020**, *1*, 3357. [CrossRef]
6. Ming, L.; Ngar, C.L. Increasing Human-Perceived Heat Stress Risks Exacerbated by Urbanization in China: A Comparative Study Based on Multiple Metrics. *Earth's Future* **2021**, *9*, e2020EF001848. [CrossRef]
7. Zhou, Z.Y.; Wang, T.; Chen, Y.Z.; Sun, Y.F.; Lu, J.Z. Spatiotemporal variations of cold waves and regional extreme low temperature along the Middle Route of South-to-North Water Transfers Project. *South-to-North Water Transf. Water Sci. Technol.* **2023**, *21*, 1098–1108. [CrossRef]
8. Gao, W.H.; Huang, Y.P.; Li, W.D.; Fu, J.X.; Li, Z. Extreme temperature change in Hekouzhen-Longmen Region and the relationship with the main atmospheric and ocean circulation patterns in 1960–2019. *Water Resour. Hydropower Eng.* **2022**, *53*, 24–37. [CrossRef]
9. Zhao, M.Y. Study on runoff changes in the Minghe River Basin under the background of climate change. *Hydro Sci. Cold Zone Eng.* **2023**, *6*, 52–55.
10. Yang, Y.; Zhao, N.; Yue, T.X. Spatio-temporal Variations of Extreme High Temperature Event in China From 1980 to 2018. *Sci. Geogr. Sin.* **2022**, *42*, 536–547. [CrossRef]
11. Guo, Y.; Gasparrini, A.; Armstrong, B.G.; Tawatsupa, B.; Tobias, A.; Lavigne, E.; Pan, X.C.; Kim, H.; Hashizume, M.; Tian, L.W.; et al. Heat wave and mortality: A multicounty, multicommodity study. *Environ. Health Perspect.* **2017**, *125*, 087006. [CrossRef]
12. Diaz, J.; Carmona, R.; Miron, I.J.; Luna, M.Y.; Linares, C. Time Trend in the Impact of Heat Waves on Daily Mortality in Spain for a Period of over Thirty Years (1983–2013). *Environ. Int.* **2018**, *116*, 10–17. [CrossRef]
13. Liu, R.Z.; Ma, X.Y.; Zhao, H.Y.; Wang, W.C.; Qin, P.P.; Yang, J.; Cheng, B.W. Health Effects of Extreme Low Temperatures and Cold Waves on Respiratory Diseases. *Biomed. Environ. Sci.* **2024**, *37*, 682–685. [CrossRef]
14. Fisher, J.A.; Jiang, C.; Soneja, S.I.; Mitchell, C.; Puett, R.C.; Sapkota, A. Summertime Extreme Heat Events and Increased Risk of Acute Myocardial Infarction Hospitalizations. *J. Expo. Sci. Environ. Epidemiol.* **2017**, *27*, 276–280. [CrossRef]
15. Wu, J.L. *The Correlation of Temperature and Cold Wave with Non-Accidental Death and the Cross-Case Study of Death Burden in Tibet Plateau*; Southern Medical University: Guangzhou, China, 2022. [CrossRef]
16. Wang, Y.; Lu, B.; Han, Z. Rapid Increase of the Nighttime Electricity Demand in Beijing Due to Compound Heatwaves. *Urban Clim.* **2023**, *50*, 101595. [CrossRef]
17. Gabbe, C.J.; Pierce, G. Extreme Heat Vulnerability of Subsidized Housing Residents in California. *Hous. Policy Debate* **2020**, *30*, 843–860. [CrossRef]
18. Kong, F. Coordinating and Promoting Global Climate Governance to Facilitate Addressing Extreme Hot Weather Disasters. *Overv. Disaster Prev.* **2023**, *4*, 4–11.
19. Mbawala, J.R.; Li, H.X.; Ndabagenga, D.M.; Zeng, J.N. Mlonganlie. Assessment of the Spatio-Temporal Trends of Annual Extreme Temperature Indices over Tanzania during the Period of 1982–2022. *J. Geosci. Environ. Prot.* **2024**, *12*, 33–50. [CrossRef]
20. Zaharaddeen, I.; Ajiya, B.S.; Abdussalam, A.F.; Muktar, I.; Babati, A.H.; Mustapha, B.B.; Yunusa, U.A. Impact of climate change on climate extreme indices in Kaduna River basin, Nigeria. *Environ. Sci. Pollut. Res. Int.* **2023**, *30*, 77689–77712. [CrossRef]
21. Zúñiga, L.M.; Huarte, B.R.; Regoto, P.; Torrez, L.; Olmo, M.; Lyra, A.; Quispe, P.D.; Bettolli, L.M. Extreme indices of temperature and precipitation in South America: Trends and intercomparison of regional climate models. *Clim. Dyn.* **2022**, *62*, 4541–4562. [CrossRef]
22. Carla, M.; Aaron, P. Long-term trends in daily extreme air temperature indices in Ireland from 1885 to 2018. *Weather Clim. Extrem.* **2022**, *36*, 100464. [CrossRef]
23. Jiang, R.G.; Li, W.; Lu, X.X.; Xie, J.C.; Zhao, Y.; Li, F.W. Assessment of temperature extremes and climate change impacts in Singapore, 1982–2018. *Singap. J. Trop. Geogr.* **2021**, *42*, 378–396. [CrossRef]
24. Alexander, L.V.; Zhang, X.; Peterson, T.C.; Caesar, J.; Gleason, B.; Haylock, M.; Collins, D.; Trewin, B.; Rahimzadeh, F.; Tagipour, A.; et al. Global observed changes in daily climate extremes of temperature and precipitation. *J. Geophys. Res. Tmospheres* **2006**, *111*, 1042–1063. [CrossRef]
25. Lucas, E.W.M.; Sousa, F.A.S.; Silva, F.D.S.; Rocha, J.R.L.; Pinto, D.D.C.; Silva, V.P.R. Trends in climate extreme indices assessed in the Xingu River basin-Brazilian Amazon. *Weather Clim. Extrem.* **2021**, *31*, 100306. [CrossRef]
26. Brown, S.J.; Ceaser, J.; Ferro, C.A.T. Global changes in extreme daily temperature since 1950. *J. Geophys. Res. Atmos.* **2008**, *113*, D05115. [CrossRef]
27. Kalyan, A.; Ghose, D.K.; Thalagapu, R.; Guntu, R.K.; Agarwal, A.; Kurths, J.; Rathinasamy, M. Multiscale spatiotemporal analysis of extreme events in the Gomati River Basin, India. *Atmosphere* **2021**, *4*, 480. [CrossRef]

28. Choi, G.; Collins, D.; Ren, G.Y.; Trewin, B.; Fukuda, Y.; Afzaal, M.; Pianmana, T.; Gomboluudev, P.; Lias, N.; Kwon, W.-T.; et al. Changes in Means and Extreme Events of Temperature and Precipitation in the Asia-Pacific Network Region, 1955–2007. *Int. J. Climatol.* **2009**, *29*, 1906–1925. [CrossRef]
29. Almazroui, M.; Islam, M.N.; Dambulla, R.; Jones, P.D. Trends of Temperature Extremes in Saudi Arabia. *Int. J. Climatol.* **2014**, *34*, 808–826. [CrossRef]
30. Aguilar, E.; Peterson, T.C.; Obando, P.R.; Frutos, R.; Retana, J.A.; Soley, J.; Araujo, R.M.; Santos, A.R.; Valle, V.E.; Brunet, M.; et al. Changes in Precipitation and Temperature Extremes in Central America and Northern South America, 1961–2003. *J. Geophys. Res. Atmos.* **2005**, *110*, D23. [CrossRef]
31. Zhang, N.; Sun, Z.B.; Zeng, G. Changes of extreme temperature in China from 1955 to 2005. *J. Nanjing Inst. Meteorol.* **2008**, *31*, 123–128. [CrossRef]
32. Chen, Y.; Zhai, P.M.; Zhou, B.Q. Detectable Impacts of the Past Half-Degree Global Warming on Summertime Hot Extremes in China. *Geophys. Res. Lett.* **2018**, *45*, 7130–7139. [CrossRef]
33. Zheng, W.; Si, W.Y.; Du, Z.Q.; Wu, Z.T.; Liang, H.X. Spatial and temporal patterns of summer heatwaves in northern China from 1961 to 2020. *J. Shanxi Univ. (Nat. Sci. Ed.)* **2024**, 1–10. [CrossRef]
34. Zhang, S.Q.; Ren, G.Y.; Zheng, X.; He, J.J.; Sun, X.B.; Ren, Y.Y.; Xue, X.Y.; Yang, G.W. Changes in the mean and extreme temperature in the Yangtze River Basin over the past 120 years. *Weather Clim. Extrem.* **2023**, *40*, 100557. [CrossRef]
35. Zhang, C.J.; Xiao, C.; Li, S.; Zhujie, S.B.; Ren, Y.Y.; Zhang, S.Q.; Wang, R. Construction of comprehensive risk level index of extreme climate events and comprehensive analysis of extreme climate in the Yangtze River Basin in recent 60 years. *Chin. J. Geophys.* **2023**, *66*, 920–938.
36. Sun, W.H.; Han, L.; Liu, X.Y. Spatial and temporal distribution characteristics of extreme temperature events in Sichuan Province from 1969 to 2019. *Water Resour. Hydropower Eng.* **2023**, *54*, 113–127. [CrossRef]
37. Gegen, B.T.; Wei, W.; Zhang, X.; Yang, X.H.; Shi, Z.J. Spatiotemporal trends and periodic features of climate extremes over the Qaidam Basin, China, during 1960–2014. *Arid. Zone Res.* **2020**, *37*, 304–313. [CrossRef]
38. Yin, H.; Sun, Y. Analysis of Extreme Temperature and Precipitation Characteristics in China Based on ETCCDI Index in 2017. *Prog. Clim. Change Res.* **2019**, *15*, 363–373.
39. You, Q.L.; Jiang, Z.H.; Kong, L.; Wu, Z.W.; Bao, Y.T.; Kang, S.C.; Pepin, N. A comparison of heat wave climatologies and trends in China based on multiple definitions. *Clim. Dyn.* **2017**, *48*, 3975–3989. [CrossRef]
40. Mukherjee, S.; Mishra, V. A sixfold rise in concurrent day and night-time heatwaves in India under 2 °C warming. *Sci. Rep.* **2018**, *8*, 16922. [CrossRef]
41. Gosling, S.N.; Lowe, J.A.; McGregor, G.R.; Pelling, M.; Malamud, B.D. Associations between elevated atmospheric temperature and human mortality: A critical review of the literature. *Clim. Change* **2009**, *92*, 299–341. [CrossRef]
42. Gao, D.Y.; You, R.Y.; Zhu, H.; Zhang, X.; Tan, F.L. Spatiotemporal variation characteristics of extreme precipitation in Sichuan Province based on RClimDex model. *Water Resour. Power* **2021**, *39*, 10–13.
43. Dunn, H.J.R.; Alexander, V.L.; Donat, G.M.; Zhang, X.B.; Bador, M.; Herold, N.; Lippmann, T.; Allan, R.; Aguilar, E.; Barry, A.A.; et al. Development of an Updated Global Land in Situ-Based Data Set of Temperature and Precipitation Extremes: HadEX3. *J. Geophys. Res. Atmos.* **2020**, *125*, e2019JD032263. [CrossRef]
44. Yang, W.T.; Sun, J.G.; Kang, Y.T.; Ma, H.L.; Xu, R.Z. Temporal and spatial changes of extreme climate index in the Loess Plateau. *Arid. Land Geographys.* **2019**, *43*, 1456–1466.
45. Ya, R.; Li, N.; Yin, S.; Bao, Y.H. Characteristics of temporal and spatial variation of extreme climate events in Inner Mongolia during the period 1960–2015. *Res. Soil Water Conserv.* **2020**, *27*, 106–112. [CrossRef]
46. Cohen, I.; Huang, Y.; Chen, J.; Benesty, j. Pearson correlation coefficient. *Noise Reduct. Speech Process.* **2009**, *2009*, 1–4. [CrossRef]
47. Saadia, Z. *The Global Risks Report 2024*, 19th ed.; World Economic Forum: Geneva, Switzerland, 2024; pp. 1–121.
48. Cheng, Q.; Yang, B.Y.; Jia, C.J.; Zhong, Y.Y.; Zhang, Y.T.; Pinto, L.; Huang, C.R.; Li, S.H.; Wei, K. Rapid attribution of the record-breaking heatwave event in North China in June 2023 and future risks. *Environ. Res. Lett.* **2024**, *19*, 014028. [CrossRef]
49. Wang, X.Y.; Li, Y.Q.; Yan, M.; Gong, X.W. Changes in temperature and precipitation extremes in the arid regions of China during 1960–2016. *Front. Ecol. Evol.* **2022**, *10*, 902813. [CrossRef]
50. Wang, X.L. *Variation of Extreme Climate and Its Impact on NDVI in the Coastal Area of China*; Yantai Institute of Coastal Zone Research, Chinese Academy of Sciences: Yantai, China, 2017.
51. Zhang, J.Y.; Qian, C. Linear Trends in Occurrence of High Temperature and Heat Waves in China for the 1960–2018 Period: Method and Analysis Results. *Clim. Environ. Res.* **2020**, *25*, 225–239. (In Chinese)
52. Cao, Q.; Hao, Z.C.; Fu, X.J.; Hao, J.; Lu, C.Y. Spatiotemporal changes of extreme climatic elements in China during 1960–2017. *Yellow River* **2019**, *42*, 11–17.
53. Chen, Y.; Zhai, P. Revisiting summertime hot extremes in China during 1961–2015: Overlooked compound extremes and significant changes. *Geophys. Res. Lett.* **2017**, *44*, 5096–5103. [CrossRef]
54. Mahlstein, I.; Hegerl, G.; Solomon, S. Emerging local warming signals in observational data. *Geophys. Res. Lett.* **2012**, *39*, L21711.
55. Fan, L.L.; Du, L. Combined effects of climatic fac-tors on extreme sea level changes in the Northwest Pacific Ocean. *Ocean Dyn.* **2023**, *73*, 181–199. [CrossRef]
56. Zhu, H.H.; Jang, Z.H.; Li, L. Projection of climate extremes in China, an incremental exercise from CMIP5 to CMIP6. *Sci. Bull.* **2021**, *66*, 2528–2537. [CrossRef] [PubMed]

57. Liu, D.C.; Li, Y.; Wang, P.F.; Zhong, H.Q.; Wang, P. Sustainable agriculture development in northwest China under the impacts of global climate change. *Front. Nutr.* **2021**, *8*, 706552. [CrossRef] [PubMed]
58. Wu, G.P.; Zhao, Q.; Wang, X.; Chen, Y.L.; Zhang, Y.H. Extreme climate change and its relationship with atmospheric circulation in the Haihe River Basin from 1961 to 2020. *J. Water Resour. Water Eng.* **2024**, *35*, 100–110.
59. Su, Y.; Lu, C.Y.; Huang, Y.F.; Su, Y.L.; Wang, Z.L.; Lei, Y.F. Quantitative Analysis of Spatio-temporal Evolution Characteristics of Seasonal Average Maximum Temperature and Its Influence by Atmospheric Circulation in China from 1950 to 2019. *Environ. Sci.* **2023**, *44*, 3003–3016. [CrossRef]
60. Gao, T.; Luo, M.; Lau, N.C.; Chan, T.O. Spatially distinct effects of two El Niño types on summer heat extremes in China. *Geographys. Res. Lett.* **2020**, *47*, e2020GL086982. [CrossRef]
61. Liu, Q.; Zhou, T.J.; Mao, H.T.; Fu, C.B. Decadal variations in the relationship between the western Pacific subtropical high and summer heat waves in East China. *J. Clim.* **2019**, *32*, 1627–1640. [CrossRef]
62. Deng, K.Q.; Yang, S.; Ting, M.F.; Zhao, P.; Wang, Z.Y. Dominant modes of China summer heat waves driven by global sea surface temperature and atmospheric internal variability. *J. Clim.* **2019**, *32*, 3761–3775. [CrossRef]